PHILOSOPHICAL TRANSACTIONS OF THE ROYAL SOCIETY A

CrossMark click for updates

Phil. Trans. R. Soc. A (2012) **370**, 4904–4926
doi:10.1098/rsta.2012.0202

Review

Termination control of electronic phases in oxide thin films and interfaces: $LaAlO_3/SrTiO_3(001)$

By R. Pentcheva[1,*], R. Arras[1], K. Otte[1], V. G. Ruiz[1] and W. E. Pickett[2]

[1]*Department of Earth and Environmental Sciences, Section Crystallography and Center of Nanoscience, University of Munich, Theresienstrasse 41, 80333 Munich, Germany*
[2]*Department of Physics, University of California, Davis, One Shields Avenue, Davis, CA 95616, USA*

A wealth of intriguing properties emerge in the seemingly simple system composed of the band insulators $LaAlO_3$ and $SrTiO_3$ such as a two-dimensional electron gas, superconductivity and magnetism. In this paper, we review the current insight obtained from first principles calculations on the mechanisms governing the behaviour of thin $LaAlO_3$ films on $SrTiO_3(001)$. In particular, we explore the strong dependence of the electronic properties on the surface and interface termination, the finite film thickness, lattice polarization and defects. A further aspect that is addressed is how the electronic behaviour and functionality can be tuned by an $SrTiO_3$ capping layer, adsorbates and metallic contacts. Lastly, we discuss recent reports on the coexistence of magnetism and superconductivity in this system for what they might imply about the electronic structure of this system.

Keywords: oxide interfaces; density functional theory; magnetic thin oxide films; metal–insulator transition; metal-insulator contacts; Schottky barrier

1. Introduction

The advance of thin-film growth techniques such as pulsed laser deposition (PLD) and molecular beam epitaxy allows the fabrication of single terminated oxide interfaces on the atomic scale. Understanding the novel phenomena arising in these artificial materials is not only of fundamental interest, but is also relevant for the development of future electronics and spintronics devices. A system that has attracted most of the interest so far is composed of the simple band insulators $LaAlO_3$ (LAO) and $SrTiO_3$ (STO), where a two-dimensional electron gas (2DEG) [1], superconductivity [2], magnetism [3] and even signatures of their coexistence [4–6] have been reported. A further feature of interest and potential importance is that the electronic properties can be tuned by the LAO thickness,

*Author for correspondence (rossitza.pentcheva@lrz.uni-muenchen.de).

One contribution of 10 to a Discussion Meeting Issue ‘The new science of oxide interfaces’.

and the system undergoes a transition from insulating to conducting behaviour at around four monolayers (ML) LAO [7]. This insulator–metal transition (IMT) can be controlled reversibly via an electric field, e.g. by an atomic force microscope (AFM) tip [8–10], and several electronic devices based on this feature have been proposed [11,12]. The electronic properties can be further tuned by an additional STO capping layer that triggers the IMT already at 2 ML, thereby stabilizing an electron–hole bilayer [13]. The electronic properties show a strong dependence on the growth conditions: varying the oxygen partial pressure in the PLD chamber from 10^{-6} to 10^{-3} mbar induces an increase in sheet resistance by seven orders of magnitude [3]. This enormous change implies that oxygen defects play a controlling role during low-pressure growth.

Extensive theoretical and experimental efforts aim at explaining the origin of these interfacial phenomena. A central feature is the polar discontinuity that emerges at the interface: in the (001) direction, LAO consists of charged $(LaO)^+$ and $(AlO_2)^-$ planes, while in STO, formally neutral $(SrO)^0$ and $(TiO_2)^0$ planes alternate. Because both cations change across the interface, two distinct interfaces can be realized: an electron-doped n-type with an LaO layer next to a TiO_2 layer and a hole-doped p-type interface with an SrO and AlO_2 next to each other. Assuming formal ionic charges, the electrostatic potential produced by an infinite stack of charged planes would grow without bounds, a phenomenon known as the *polar catastrophe* [14,15]. This polar catastrophe cannot of course actually occur, and it may be avoided in several ways: a mechanism also common to semiconductors is an *atomic reconstruction* via introduction of defects or adsorbates. In transition metal oxides, electronic degrees of freedom may lead to an alternative compensation mechanism, i.e. an *electronic reconstruction*. The latter can give rise to exotic electronic states—for example, the observed 2D conductivity in LAO/STO, charge/spin/orbital order, excitonic or superconducting phases. A further question that arises is whether a thin film of LAO with only a few layers approaches the regime of the *polar catastrophe*. Sorting out the many possibilities is challenging owing to the strong dependence on growth method and conditions.

In this paper, we review the progress made so far in understanding the mechanisms that determine the electronic behaviour of LAO/STO(001) based on density functional theory (DFT) calculations. For further reviews on the experimental and theoretical work, the reader is referred to Pauli *et al.* [16], Huijben *et al.* [17], Pentcheva & Pickett [18], Chen *et al.* [19] and Zubko *et al.* [20]. In particular, we address finite size effects and the role of electrostatic boundary conditions [21] in thin LAO films on STO(001). We first discuss intrinsic mechanisms that arise at defect-free n- and p-type interfaces providing a possible explanation for the thickness-dependent IMT. Moreover, we explore the effect of the surface termination on the band diagram. In §§3 and 5, we address the role of an STO capping layer and a metallic electrode. A controversially discussed issue is the presence of an internal potential build-up within the LAO film, as predicted by DFT calculations on LAO/STO(001) with abrupt interfaces. While recent AFM experiments provide evidence for such an internal field in terms of a polarity-dependent asymmetry of the signal [22], X-ray photoemission studies [23–25] have not been able to detect shifts or broadening of core-level spectra that would reflect an internal electric field. This discrepancy implies that besides the electronic reconstruction, extrinsic effects play a role, e.g. oxygen defects [26,27],

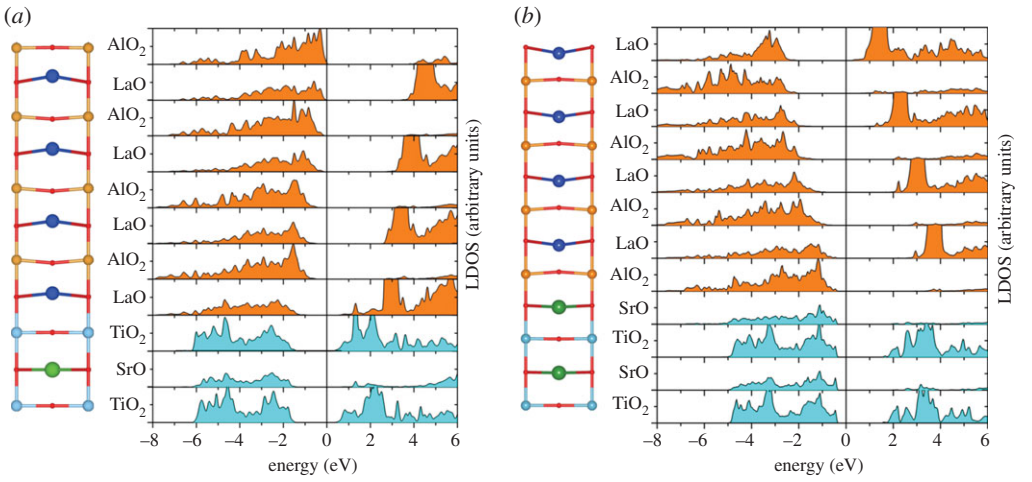

Figure 1. Side view of the relaxed structure and layer-resolved density of states (LDOS) of 4LAO/STO(001) with an (*a*) n-type and (*b*) p-type interface. Note the emergence of a potential build-up and a lattice polarization within the LAO film of opposite sign for the n- and p-type interface. (Online version in colour.)

adsorbates such as water or hydrogen [28] or cation disorder [29,30]. An overview of the current theoretical understanding of the role of such extrinsic mechanisms is provided in §4. Finally, in §6, we address recent reports on the coexistence of superconductivity and ferromagnetism in LAO/STO—a phenomenon that may be helpful in understanding the underlying electronic structure in these nanoscale systems.

2. Polar oxide films on a nonpolar substrate: $LaAlO_3/SrTiO_3(001)$

An intriguing experimental finding in LAO/STO(001) is the thickness-dependent IMT in thin LAO films on STO(001) [7]. DFT calculations demonstrate that an internal electric field emerges in thin polar LAO overlayers on STO(001) [18,31–33]. As shown in the layer-resolved density of states (LDOS) of a 4 ML LAO film on STO(001) with an n-type interface (figure 1*a*), this is expressed in an upward shift of the O 2p bands as they get closer to the surface. Interestingly, a large electric field of opposite sign arises in an analogous manner in a defect-free 4 ML LAO/STO(001) overlayer with a p-type interface (figure 1*b*). The internal electric field of the polar LAO film is screened to a large degree (but not completely) by a strong lattice polarization. As can be seen from the side view of the relaxed structure in figure 1*a* and the anion–cation buckling displayed in figure 2, for an n-type interface, this lattice polarization is characterized by a strong outward shift of La by 0.2–0.3 Å and buckling in the subsurface AlO_2 layers, while the surface layer shows similar relaxations for anions and cations. Experimental evidence for an internal electric field within the LAO film seems contradictory. Segal *et al.* [23] and Chambers *et al.* [25] found no evidence for the expected core-level shifts due to an internal field. However, evidence for a lattice polarization as a response to an internal electric field has been obtained from

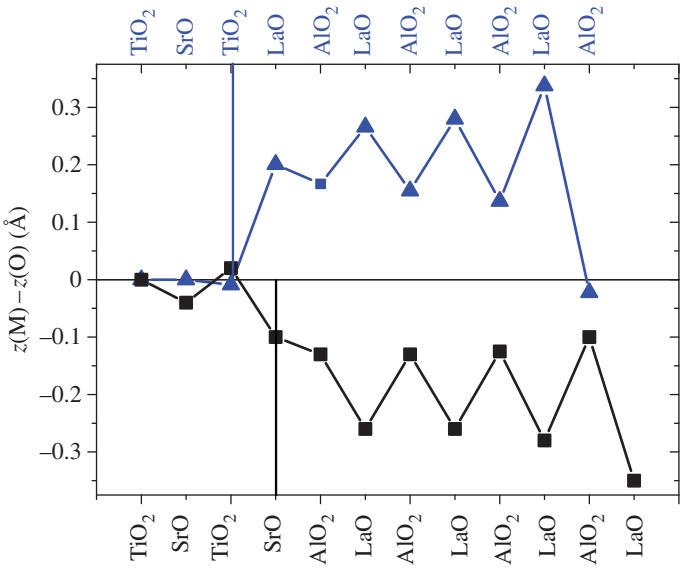

Figure 2. Oxygen–cation buckling in 4LAO/STO(001) with an n- (triangles) and a p-type interface (squares). As already shown in the side view in figure 1, the lattice polarization has an opposite sign for the n- and p-type interfaces. (Online version in colour.)

surface X-ray diffraction (SXRD) by Pauli *et al.* [34]. The latter study detected also a dependence of the lattice response on the LAO thickness with a maximum buckling in a 2 ML LAO film. This indicates possibly a stronger role of cation interdiffusion or higher affinity for adsorbates in the thicker films. Such extrinsic mechanisms can reduce the internal potential and thereby the lattice polarization (see discussion in §4).

The lattice relaxation has a crucial effect on the electronic properties: if the atoms are fixed at their ideal bulk positions, all systems are metallic [32]. The lattice polarization in the relaxed system allows several layers of LAO to remain insulating with a band gap of 1.7 eV for 1 ML LAO/STO(001) and a gradual decrease by ~ 0.4 eV per added LAO ML. Finally, at around 5 ML of LAO, an electronic reconstruction takes place. However, the closing of the band gap is *indirect* in real space, as it is due to the overlap of the valence band defined by the O 2p band in the surface layer and the conduction band marked by Ti 3d states at the interface. Consequently, the carrier density is much lower than the one expected if 0.5e were transferred to the interface. Furthermore, the results suggest carriers of two different types: electrons at the interface and holes in the surface layer. We will return to the possibility of excitonic effects later when discussing the role of an STO capping layer in §3.

For a defect-free 4LAO/STO(001) with a p-type interface, the ionic relaxations are of similar magnitude but of opposite sign (note the inward relaxation of the La ions and the anion cation buckling shown in figure 2). A very similar thickness-dependent insulator-to-metal transition is expected, which involves different states: La 5d states in the surface LaO layer and O 2p states at the interface. In experiments, the p-type interface has been found so far insulating [1] and has therefore attracted much less attention. The analysis of O K-edge spectra

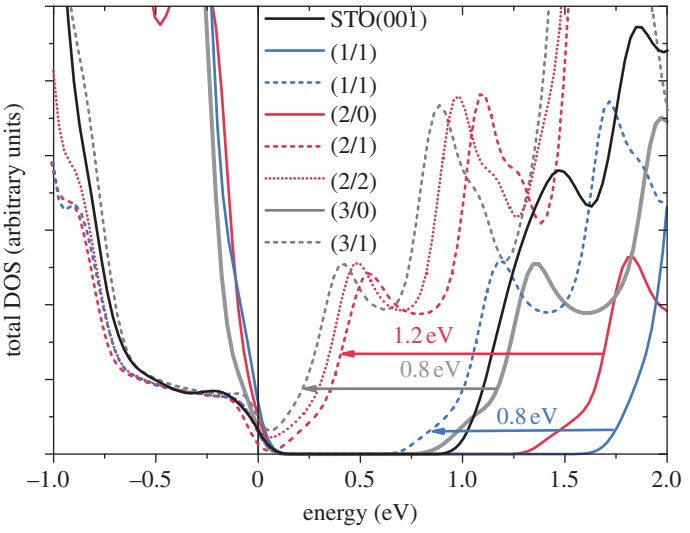

Figure 3. Total density of states (DOS) nLAO/STO(001), capped by m STO layers. Note that the band gap closes for $n > 2$ ML as soon as a capping STO layer is added. Thereby, the effect of the first STO layer is most pronounced. (Online version in colour.)

by Nakagawa *et al.* [35] suggested that compensation takes place via oxygen vacancies, that is, by atomic reconstruction. Still, the results above and those by Ishibashi & Terakura [31] show that provided defect-free LAO/STO interfaces with a p-type interface can be realized, they would exhibit just as interesting thickness-dependent properties as the ones for the n-type interface.

So far, we have considered stoichiometric 4 ML LAO films on STO(001), where, e.g. for an n-type interface, the LAO film is terminated by an AlO_2 surface layer. Pavlenko & Kopp [36] recently investigated LAO/STO(001) with an n-type interface and an LaO surface termination. Note that, here, both the surface and the interface are electron doped. Not surprisingly, the system is found to be metallic for 2.5 and 3.5 ML LAO with finite occupation of Ti $3d_{xy}$ states in the interface layer and La $5d_{x^2-y^2}$ states in the surface layer. The authors interpreted the surface La 5d occupation as a result of surface tensile stress. While the latter influences, e.g. the vertical relaxation of ions, the polarity discontinuity at the surface and interface is likely to be the dominating effect.

3. Influence of an $SrTiO_3$ capping layer

In contrast to the sharp IMT in LAO films on STO, Huijben *et al.* [37] observed a much smoother transition from insulating to conducting behaviour that starts already at 2 ML LAO if the latter is covered by a non-polar STO layer. The total DOS of n ML LAO/STO(001) covered by m layers of STO [denoted in the following as (n/m)] is displayed in figure 3. The DFT results reveal that for $n = 2$ ML, already a single STO capping layer leads to an IMT. Increasing the number of STO capping layers m or LAO layers n enhances the DOS at the Fermi level, but the first STO capping layer has the most dramatic effect, reducing the band gap by ~ 1.0 eV.

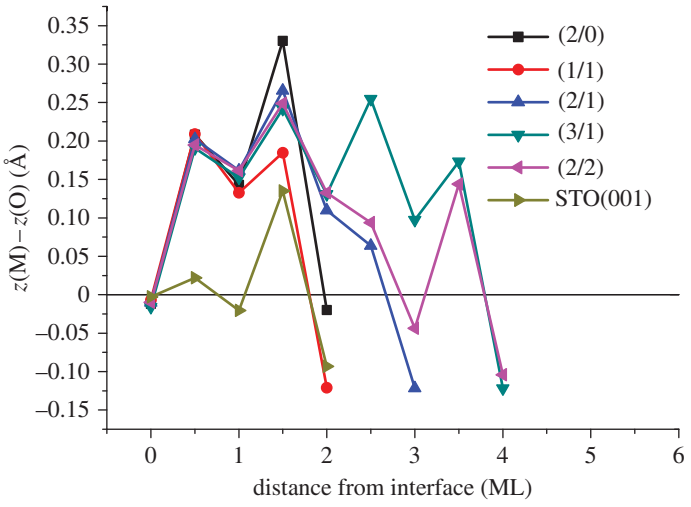

Figure 4. Cation–anion vertical buckling in mSTO/nLAO/STO(001) and at the STO(001) surface for comparison. (Online version in colour.)

In order to gain more insights into the mechanism of closing of the gap, we analyse first the lattice relaxations. Figure 4 shows the cation–anion displacements in mSTO/nLAO/STO(001). We observe slight reduction in the buckling within the LAO film compared with the (2/0) system and a polarization within the STO layer. The relaxation pattern in the STO capping layer is in fact similar to the one of the STO(001) surface [38] (for comparison, the relaxations at an STO(001) surface are added to figure 4). However, the total contribution of the STO capping layer is small as the ionic dipole moments of the SrO and TiO_2 layers are of opposite sign (negative dipole moment in the surface TiO_2 layer and a positive one in the subsurface SrO layer) and nearly cancel. The results show that the ionic contribution to the dipole moment in mSTO/nLAO/STO(001) scales with the number n of LAO layers and increases roughly by 1 eÅ per added LAO layer.

The impact of the STO capping layer turns out to be of electronic origin: Figure 5 shows the LDOS of (2/0) (dashed line) and (2/1) (solid line) lines aligned at the bottom of the Ti 3d band at the interface. In both the capped and the uncapped system, the O 2p bands within the LAO film exhibit a gradual upward shift of 0.4 eV per LAO as they approach the surface. In the capped system, there is an additional strong shift/broadening of the O 2p band in the surface TiO_2 layer of ~ 0.8 eV that closes the band gap and induces an electronic reconstruction [13].

Indeed, the band structure in figure 6*b* shows that, once the STO capping layer is added, a dispersive O 2p surface band appears similar to a surface state in STO(001) [38,39]. This band extends 0.8 eV above the subsurface O 2p band and marks the top of the valence band at the M point of the Brillouin zone. On the other hand, the bottom of the conduction band lies at the Γ point and is determined by Ti 3d states in the interface layer. Thus, the closing of the band gap is indirect in both real and reciprocal space. Increasing the number of LAO and STO capping layers enhances the overlap of the valence and conduction bands at the Fermi level.

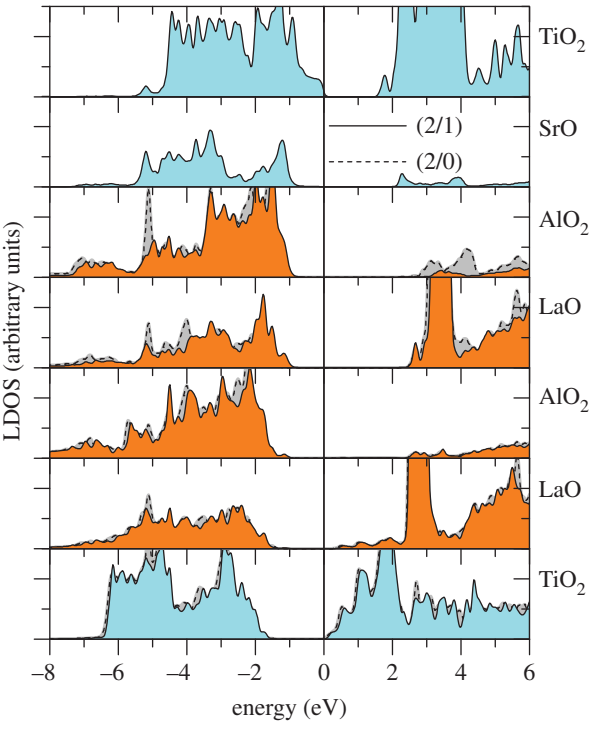

Figure 5. Layer-resolved density of states (LDOS) of 2LAO/STO(001) with (solid line) and without (dashed line) a single STO capping layer. A dispersive O 2p band in the surface TiO_2 layer leads to a closing of the band gap in the capped system [13]. (Online version in colour.)

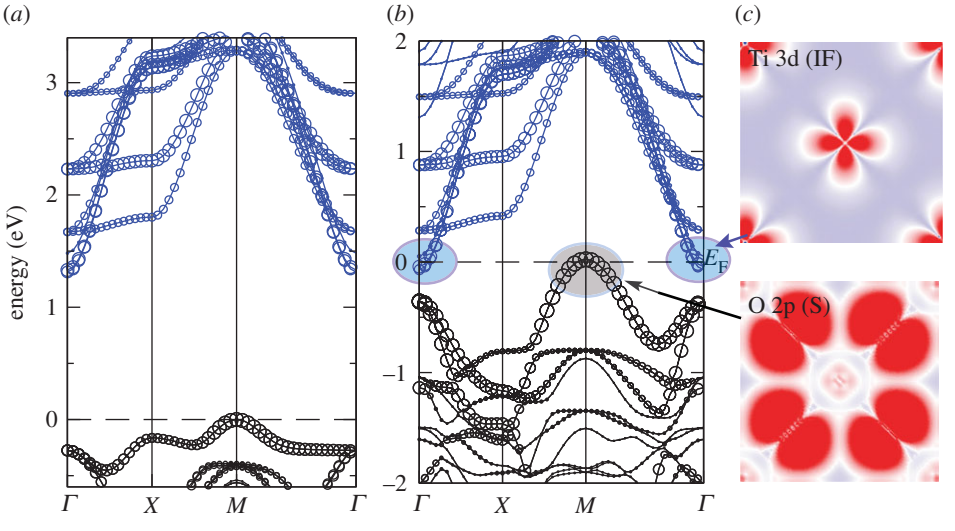

Figure 6. Band structure of (*a*) 2LAO/STO(001) with an indirect band gap and (*b*) 2STO/2LAO/STO(001) with a closed band gap due to the overlap of an electron band at Γ and a holes band at M; (*c*) integrated electron density around the Fermi level shows electrons of Ti $3d_{xy}$ character at the interface (IF) at Γ and holes of O $2p_\pi$ type at the surface (S) M. Adapted from Pentcheva *et al.* [13]. (Online version in colour.)

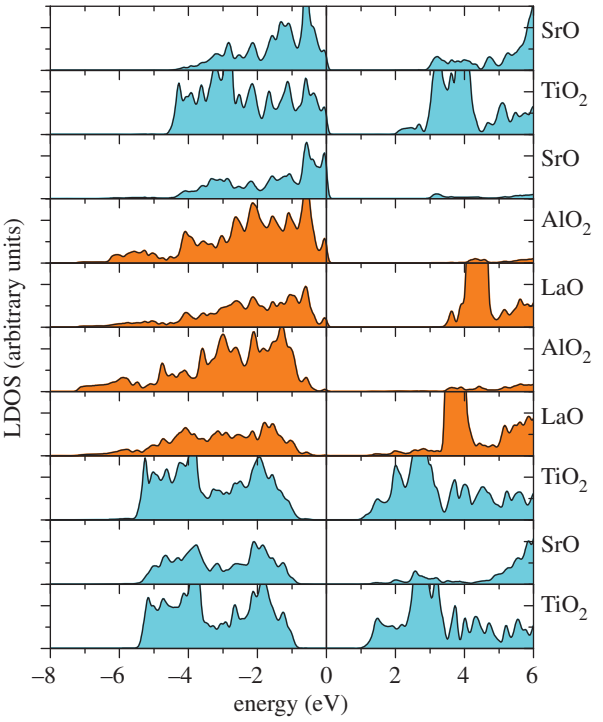

Figure 7. Layer-resolved density of states (LDOS) of an SrO terminated 1.5 ML STO/2LAO/STO(001), showing insulating behaviour. (Online version in colour.)

The electron density distribution in 2STO/2LAO/STO(001) integrated between −0.3 and 0 eV shows electrons of Ti $3d_{xy}$ character in the interface layer and holes in the O $2p_{\pi}$ bands at the surface. From the curvature of the electron and hole bands at the Γ and M points, we determine a significantly higher effective mass of the holes ($1.4\,m_e/1.2\,m_e$ in the uncapped/capped system, respectively) than for the lighter electrons ($0.4\,m_e$). The presence of two types of carriers with different mobilities is confirmed in Hall and magnetoresistance measurements [13], where the data between 0 and 100 K can be fitted only by using a two-band model with one hole and one electron band. Photoemission experiments give further evidence for the presence of holes in the surface layer [13]. Thus, the presence of a non-polar oxide capping layer seems to stabilize the system with respect to surface defects and adsorbates that are likely to eliminate holes in the uncapped systems.

In contrast, when the system is terminated by an SrO layer (using a 1.5 ML STO overlayer), the LDOS in figure 7 shows that the band gap of ~ 1 eV of the uncapped (2/0) system is preserved. The reduction of the band gap is solely due to the potential build-up within the LAO film, while the valence band (VB) of the STO capping layer aligns with the VB in the top AlO_2 layer without the surface state characteristic of the TiO_2-terminated capping layer. This system exhibits a behaviour that is closer to what one would expect when adding a 'non-polar' oxide overlayer on top of LAO/STO(001).

4. Role of lattice defects and adsorbates

(a) Cationic intermixing

The systems considered so far contained abrupt interfaces. However, several studies suggest significant cation intermixing at the interface [29,30,34]. Intermixing has been discussed as an alternative mechanism to the electronic reconstruction to compensate polarity, but the role of intermixing in cancelling the potential divergence is questioned [40]. Qiao *et al.* [30] proposed as main sources of defects the deviations from a 1:1 La:Sr ratio due to strong angular dependence during the PLD process, Sr vacancy formation and La interdiffusion into the STO substrate. They investigated La→Sr and Al→Ti substitution both near and far from the interface, using up to 4 ML LAO on a 6 ML thick STO substrate in a $c(2 \times 2)$ lateral unit cell. The DFT results indicate that coupled La–Sr, Al–Ti exchange processes involving both the surface and interface region lower the energy of the system, and the energy gain is dependent on the LAO thickness, being ~ 1.0 eV for $n = 3$ LAO and ~ 1.6 eV for $n = 4$ LAO layers, respectively. A comparison of the calculated and measured valence band offset was used as a further criterion to prove the presence of intermixing.

Pauli *et al.* [34] performed SXRD experiments, and DFT calculations on films with thickness between 2 and 5 ML LAO. The experimental data indicated an 80% filling of the surface layer with 20% of a layer on top of that. Futhermore, the results were consistent with cation intermixing exceeding 5% throughout 3 ML around the interface layer. In contrast to the study of Qiao *et al.* [30], DFT calculations on abrupt and intermixed interfaces did not show significant differences in electronic behaviour.

(b) Oxygen defects

As mentioned in the introduction, a number of experimental studies have shown the strong influence of the oxygen partial pressure during deposition or post-deposition annealing on the transport properties. Despite its importance, there are only a few studies that have addressed the role of oxygen vacancies. Cen *et al.* [8] considered a 3 ML LAO/STO(001) with a vacancy in the surface AlO_2 layer and found a dramatic difference in the electronic properties with reduction/cancellation of the electric field within the LAO film and an accumulation of carriers at the interface, in contrast to the insulating defect-free 3 ML LAO/STO(001). Chen *et al.* [41] modelled LAO/STO superlattices with a p-type interface and observed that oxygen vacancies are repelled from the interface towards bulk STO. On the other hand, Zhong *et al.* [26] studied oxygen vacancies in an $(LAO)_m/(STO)_m$ superlattice with alternating n- and p-type interfaces. In contrast to Chen *et al.* [41], they found that the formation energy of vacancies is lowest at the p-type interface and ~ 2 eV higher at the n-type interface with a nonlinear dependence in between. Furthermore, the vacancy formation tends to be more favourable in BO_2 layers than in AO layers of the perovskite ABO_3 lattice. The formation energy at the p-type interface becomes negative with respect to the one in the STO bulk at a critical thickness $m = 3$–4 ML. The electrons released by the vacancy are transferred to the conduction band minimum at the n-type interface (which now moves below the Fermi level with a significant orbital polarization in the interface and more distant TiO_2 layers), while the

p-type interface is insulating. This result implies separation between regions where impurity scattering takes place and regions of enhanced carrier density. The authors also observed that the vacancy formation reduces the core-level shifts within the superlattice and proposed this as a possible explanation of the lacking broadening in X-ray photoemission measurements [23–25].

Zhang *et al.* [42] studied the formation of vacancies in thin LAO overlayers on STO(001) using an asymmetric setup with dipole correction, and varied the position of the vacancies within the LAO film. Note that only the Γ point was used for integration within the Brillouin zone. In systems with a p-type interface, vacancies are formed preferentially at the interface, thereby compensating the valence discontinuity and leaving the system insulating. In contrast, for systems with an n-type interface, the formation energy was significantly higher. Furthermore, vacancies tend to be formed rather in the surface LAO layer than at the interface. This has two consequences: it compensates the p-type surface AlO_2 layer and enhances the carrier density at the interface. On the basis of a phenomenological electrostatic model, Bristowe *et al.* [27] showed that there is a critical thickness for surface vacancy formation, in agreement with DFT calculations [43]. Furthermore, they proposed that surface defects generate a trapping potential for carriers whose strength depends on the LAO-film thickness.

DFT calculations [44] introducing an oxygen vacancy in the interface TiO_2 layer within a 2×1 lateral unit cell indicate spin polarization of the carriers in the Ti 3d band, and propose this as a possible explanation of the recently reported coexistence of ferromagnetism and superconductivity in the LAO/STO(001) system (see also discussion in §6). Further studies are necessary to explore lower concentrations of vacancies and other thermodynamically more stable sites for the vacancy (e.g. in the surface AlO_2 layer).

(*c*) *H adsorption*

In most of the experiments so far, the samples are exposed to air; thus, the interfacial properties can be significantly affected by adsorbates. These are considered as a possible origin of reversible writing and erasing of conducting regions on LAO/STO(001) by an AFM tip [8]. Son *et al.* [33] investigated the H adsorption using DFT and the generalized gradient approximation (GGA) [45]. They found that the adsorption energy increases with LAO thickness and that beyond a critical thickness of ~ 5 ML, the energy gain exceeds the energy needed for H_2 or H_2O dissociative adsorption. An interesting feature is the planar adsorption geometry with the H–O bond being nearly parallel to the surface reflecting a maximized overlap between the H 1s orbitals and the planar O $2p_\pi$ states. H is found to donate electrons to the STO conduction band. Furthermore, the size and sign of the internal potential build-up can be tuned by the H concentration on the surface, e.g. the latter is exactly cancelled for a (2×1) surface unit cell (this coverage corresponds to 0.5e transfer per (1×1) lateral unit cell). The impact of H adsorption bears strong parallels to the influence of a metallic contact layer on the interfacial properties that is discussed in the next section. The influence of further adsorbates such as water has not been considered so far, but needs to be addressed in order to obtain a comprehensive picture of all effects that may determine the properties of LAO/STO(001).

5. Impact of metallic contacts on the electronic properties of $LaAlO_3/SrTiO_3(001)(001)$

In §§3 and 4, we have seen that the presence of a non-polar oxide overlayer or defects can significantly alter the electronic properties of the LAO/STO system. For device applications, metallic overlayers are important, and several experimental studies have used setups with metallic contacts on LAO/STO(001) [10,46,47]. The coupling between metallic thin films and semiconductors or ferroelectric oxides have been widely studied [48–52]. In order to gain understanding of the impact of metallic contacts on the electronic behaviour of an oxide interface, we have recently performed DFT calculations on a series of metal electrodes on LAO/STO(001) [53]. Here, we discuss how the electronic properties can be influenced by the metallic contact.

All the calculations presented in this section have been performed with the full potential linearized augmented plane wave method in the WIEN2K implementation [54] using the GGA [45]. We have also explored the influence of an on-site Coulomb repulsion parameter (local density approximation/GGA + U method [55]) with $U = 5\,\mathrm{eV}$ and $J = 1\,\mathrm{eV}$ for the Ti 3d orbitals, and $U = 7\,\mathrm{eV}$ for the La 4f orbitals. The irreducible part of the Brillouin zone was sampled with 21 k-points. The systems were modelled by a symmetric slab, with a 2 and 4 ML LAO film on a TiO_2-terminated STO substrate with a lateral lattice parameter set to the GGA value of bulk STO (3.92 Å). The influence of the substrate thickness was probed by using a system with a thin (2.5 ML) and thick (6.5 ML) STO slab. The metal atoms were adsorbed on top of the oxygen atoms in the top AlO_2 layer. These sites were found to be energetically favourable in previous studies of metallic overlayers on LAO(001) [56] and for other transition metal/perovskite oxide interfaces [57–59]. Further metallic layers are deposited, assuming a face-centred cubic stacking of the layers. A vacuum of at least 10 Å was used to separate the supercell from its periodic images and avoid spurious interactions. The atomic positions were relaxed within tetragonal symmetry. A side view of the relaxed systems with an Al (1 ML), Ti (1 and 2 ML) and Pt (1 ML) overlayer is shown in figure 8.

As discussed in §2, in the nLAO/STO(001) system, a central feature is the upward shift of the O 2p bands within the polar LAO film. The LDOS of Al, Ti and Pt contact layers on top of 2 ML LAO/STO(001) are shown in figure 9. Upon adsorption of an Al or Ti overlayer, this potential build-up is largely cancelled. In contrast, for Pt, there is a non-vanishing shift of the unoccupied La 4f and 5d bands. In all cases, both the surface contact layer and the interface (IF) layer are metallic with a significant occupation of the Ti 3d band at the interface and a decreasing occupation in deeper layers.

As can be seen from the band structure in figure 10, multiple bands contribute to conductivity: the lowest lying bands at the interface are of Ti $3d_{xy}$ character, in the IF-1 layer all t_{2g} states contribute, while in deeper layers d_{xz}, d_{yz} bands lie lowest in energy. The d_{xy} bands have a strong dispersion along $M-\Gamma-X$, whereas d_{xz} and d_{yz} are heavier along $\Gamma-X$. This difference in velocities (masses) suggests different mobilities of the carriers. Further bands between E_F and $E_F - 2.0\,\mathrm{eV}$ stem from the surface metallic layer. We observe that the occupation of Ti 3d bands at the interface depends strongly on the type of metal contact on the

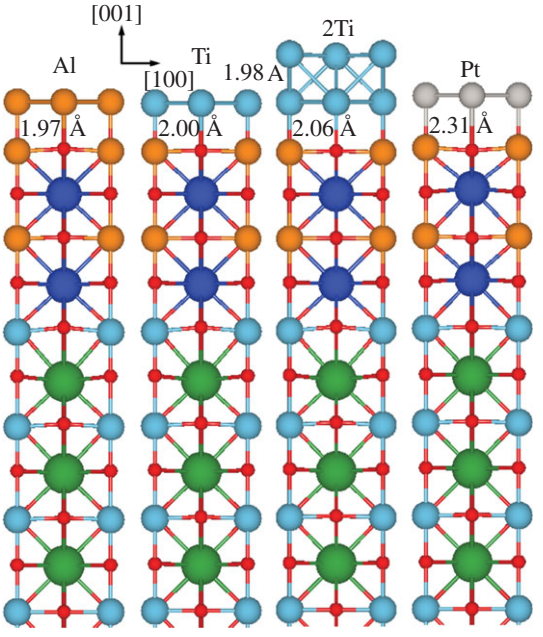

Figure 8. Side view of the relaxed structures for M/LAO/STO systems (M = Al, Ti, 2Ti and Pt). Only half of our symmetric slab is shown. M–O bond lengths near the surface increase from Al to Pt. In contrast, the buckling in the interface TiO_2 layer decreases. (Online version in colour.)

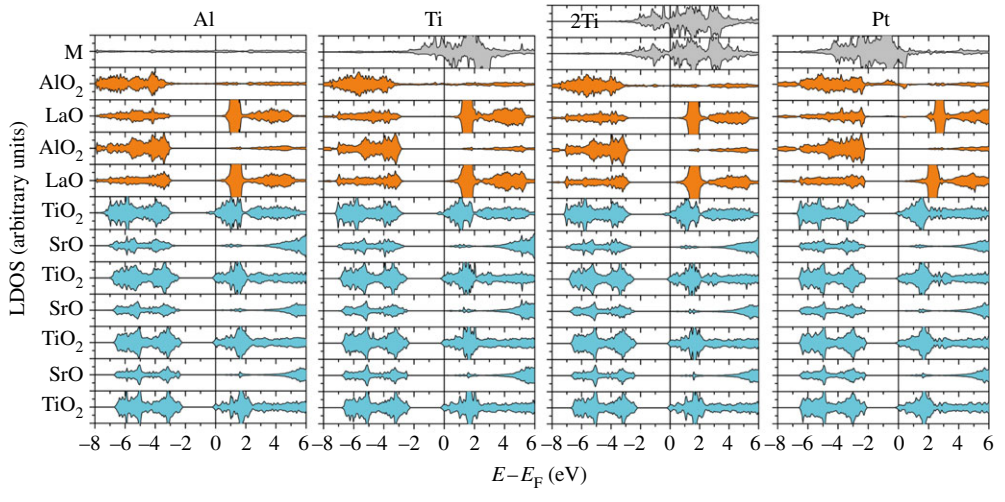

Figure 9. Layer-resolved density of states (LDOS) for 2 ML LAO/STO(001) with Al (1 ML), Ti (1 and 2 ML) and Pt (1 ML). The internal electric field, observed in the uncovered films, is cancelled for an Al and Ti contact. A residual field is obtained for a Pt electrode. (Online version in colour.)

surface: for an Al, Ti and Pt overlayer, the band edge is 0.65, 0.5 and 0.25 eV below the Fermi level at Γ.

Further insights into the influence of the contact layer on the structural and electronic properties of LAO/STO(001) can be obtained from figure 11. The buckling within the layers expressed as a relative shift of anion and cation

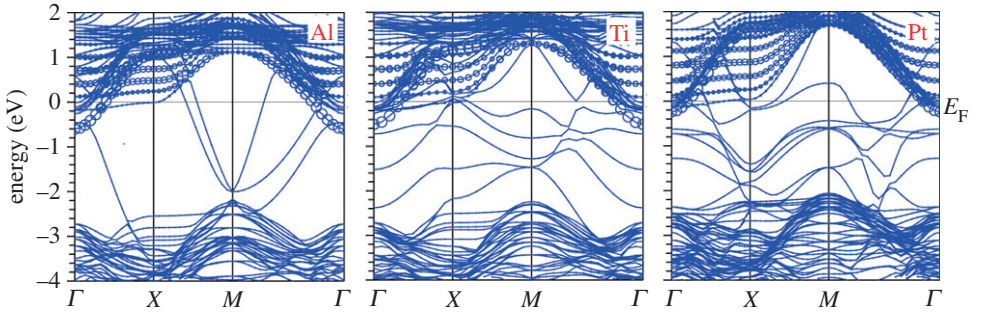

Figure 10. Majority spin band structures for M/LAO/STO systems (M = Al, Ti and Pt). The contribution of Ti 3d states from the interface TiO_2 layer is marked by circles. (Online version in colour.)

z-coordinate in figure 11 differs significantly compared with the systems without a metallic contact. As discussed in §2, in the uncovered LAO films on STO(001), the lattice polarization is confined to the LAO film where it plays a decisive role to counteract the divergence of the electric potential, while the buckling is negligible within the STO substrate (see lines with empty symbols). In contrast, after adsorbing the metallic overlayer, the potential build-up in LAO is largely cancelled and hence the anion–cation buckling is strongly reduced in size (Pt contact) and even changes sign (Al and Ti overlayer).

On the other hand, a notable polarization emerges within STO that is strongest at the interface and decays in deeper layers. The pattern is similar to the one in $LaTiO_3$/STO and LAO/STO superlattices with an n-type interface [60,61]. This lattice polarization in STO correlates directly with the occupation of Ti 3d bands (figure 11*b*), which is highest in the interface TiO_2 layer and decays in deeper layers. Concerning the chemical effects of the overlayer, the lattice polarization and band occupation at the interface are highest for the system with an Al overlayer, followed by Ti and lowest for a Pt overlayer. The position of O 1s level, which is a monitor of the local potential, shows a similar trend with the strongest binding energy in the interface TiO_2 layer for an Al contact layer. The strength in binding to the surface is reflected also in the M–O bond lengths, Al–O being the shortest (1.97 Å), followed by Ti–O (2.00 Å) and Pt–O being longest (2.31 Å) (see figure 8).

(*a*) *Dependence on the metallic contact thickness*

To investigate the dependence on the metallic contact thickness, we have varied the thickness of the Ti overlayer. The calculations for 2 ML Ti/2LAO/STO(001) show a similar occupation of the Ti 3d band at the interface but a stronger band bending in the deeper layers leading to a lower total number of electrons within STO. This correlates with a slightly larger distance between Ti in the contact layer and oxygen in the top AlO_2 layer of 2.00 Å versus 2.06 Å for 1 ML and 2 ML Ti/2LAO/STO(001), respectively.

(*b*) *Schottky barriers*

Another illuminating characteristic of the M/LAO/STO(001) system, important for understanding the variation of band lineups and in view of device

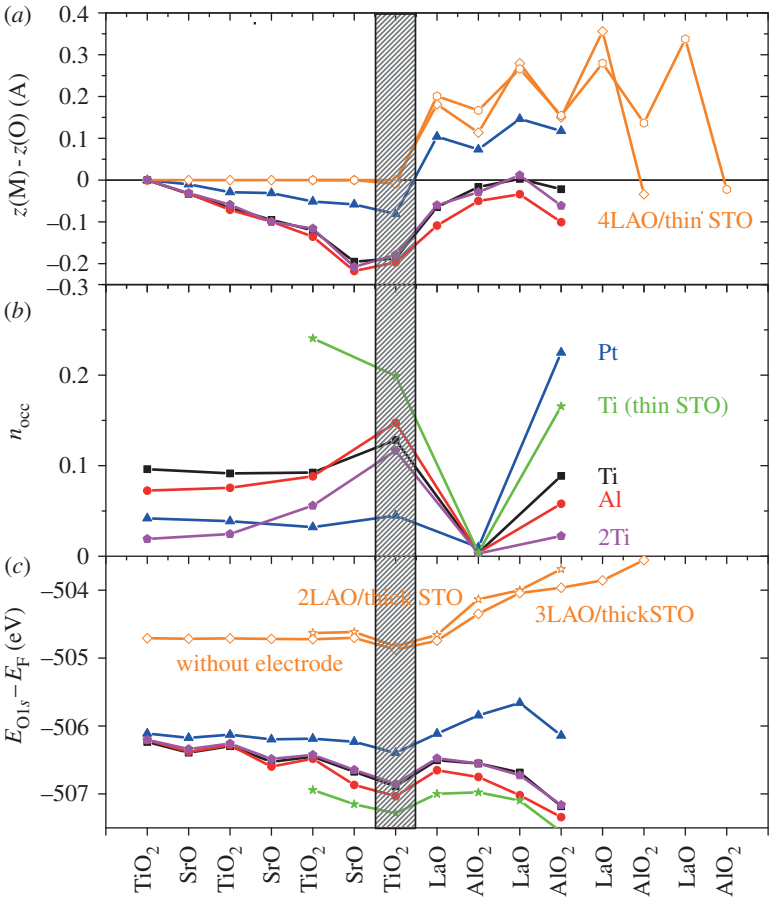

Figure 11. (*a*) Oxygen–cation buckling along the [001] direction. (*b*) Layer-resolved electron occupation integrated between $E_F - 0.65$ eV and E_F. Charge on the LaO and SrO layers is zero (not shown). (*c*) Positions of O 1s states with respect to E_F. Data for 1 ML Ti and thin/thick STO substrate is marked by stars/squares; 2 ML Ti (pentagons), as well as 1 ML Pt (triangles) and 1 ML Al (circles). Results for *n*LAO/STO(001) without a metallic overlayer are displayed with empty symbols (stars, diamonds and hexagons for $n = 2, 3, 4$ ML, respectively). (Online version in colour.)

applications, are the Schottky barrier heights (SBHs). As displayed in Table 1, these correlate with the strength of the chemical bond and, most importantly, with the work function: Al has the highest p-SBH (3.0 eV), followed by Ti (2.8 eV) and finally Pt (2.2 eV). As the well-known underestimation of band gaps within GGA is mostly related to the position of the conduction band minimum, the n-SBH tend to be too small. Taking the experimental band gap of LAO, the n-SBHs are 2.6 eV (Al), 2.8 eV (Ti) and 3.4 eV (Pt). The relevance of the chemical bonding between *M* and LAO/STO(001) is in line with previous findings for metal–oxide interfaces [62].

Figure 12 displays the schematic band diagrams of three distinct mechanisms of formation of a 2DEG in LAO/STO(001), STO/LAO/STO(001) and *M*/LAO/STO(001). For LAO/STO(001), a thickness-dependent IMT occurs as

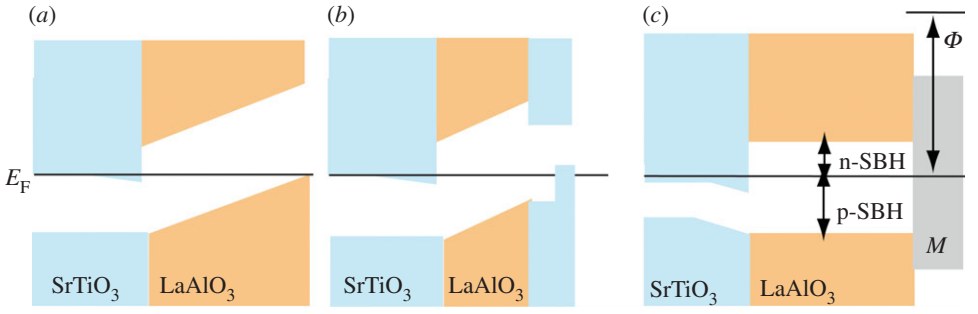

Figure 12. Schematic band diagram of (*a*) LAO/STO(001) at the verge of an electronic reconstruction at the critical LAO thickness; LAO/STO(001) covered by (*b*) an STO overlayer which leads to IMT already at 2 ML LAO and (*c*) a metallic contact layer (*M*). Note that the potential build-up that leads to an electronic reconstruction in (*a*) and (*b*) beyond a critical LAO thickness is eliminated in *M*/LAO/STO(001). (Online version in colour.)

Table 1. Calculated *M*–O bond lengths, Ti–O buckling (difference in *z*-coordinate between cations and oxygen) and Ti 3d band occupation in the interface layer, integrated between $E_F - 0.65$ eV and E_F. Work functions and Schottky barrier heights for the different contact overlayers are also displayed.

metallic layer	O–*M* distance (Å)	$z_{Ti} - z_O$ (IF) (Å)	n_{occ}	Φ (eV)	p-SBH (eV)
Al	1.97	−0.20	0.15	3.53	3.0
Ti	2.00	−0.19	0.13	4.05	2.8
2Ti	2.06	−0.18	0.11	4.05	2.8
Pt	2.31	−0.08	0.04	5.60	2.2

a result of the potential build-up within the LAO film, where the electronic reconstruction involves the formation of holes at the surface and electrons at the interface. In STO/LAO/STO(001) due to an additional surface state in the top TiO_2 layer, the IMT takes place at a much lower LAO critical thickness, leading to the formation of an electron–hole bilayer. In contrast, for *M*/LAO/STO(001) (*M* = Al, Ti), the potential in LAO is flat, regardless of the LAO or STO thickness. Simultaneously, a 2DEG with higher carrier density is formed at the interface. In the case of Pt (and other transition and noble metals, for more details see [53]), likely due to the weaker bonding and smaller charge transfer to the oxide layer, a residual slope within LAO is found, consistent with the recently measured potential build-up in Pt/LAO/STO(001) [47].

The evolution of the system due to deposition of the contact can be considered in several steps. Beginning with the internal field in 2 ML LAO/STO(001) [~ 0.8 eV potential rise], the metal layer is added and allowed to equilibrate with the outer LAO layer, determining the work function and the Schottky barrier (contact Fermi level with respect to the LAO band edges). On the basis of the final result shown in figure 9, the contact Fermi level would be ~ 1 eV above the STO conduction band minimum. Now, allowing exchange of charge with the interface—full self-consistency—electrons will flow from the contact layer to the

interface until the Fermi levels coincide. As charge is transferred, the internal field and accompanying ionic polarization decrease. The determining factor is the lineup of the surface and interface Fermi levels, which is accompanied by the (near-) disappearance of the electric field within the LAO slab. This charge transfer between the metal and the surface AlO_2 layer, leaving a slightly positive contact layer, will renormalize the work function of the metal and Schottky barrier somewhat. The self-consistent calculation gives only this final result, shown in figure 9.

(*c*) *Thin $SrTiO_3$ substrate: spin polarization*

While the results for M/LAO/STO(001) presented earlier were obtained using a 6.5 ML STO substrate, we have also performed calculations with a thin (2.5 ML) STO and observe there interesting confinement effects, which will be described later. As shown in figure 11*b*, a much higher Ti 3d band occupation is obtained at the interface for the thin STO substrate. However, the most prominent effect is a spin polarization of the 2DEG at the interface for the thin STO substrate. When adsorbing a single Ti layer, Ti displays a significant magnetic moment of $0.60\mu_B$ owing to the reduced coordination of the metal atom at the surface. We note that also a single Pt overlayer is spin polarized with $0.49\mu_B$ owing to polarization of the holes in the 5d shell. For a Ti overlayer, this effect induces a moment of 0.10 $(0.24)\mu_B$ at the Ti sites in IF (IF-1) layer. The values obtained within GGA + U, where effects of strong intra-atomic interaction are included, are enhanced: 0.20 $(0.30)\mu_B$ in IF (IF-1). Such polarization seems surprising because the interface and surface layers are separated by the insulating LAO slab, precluding (or vastly reducing) exchange coupling between the layers, but indeed the effect depends on the LAO spacer thickness. An increase in the width of the LAO layer reduces the influence of the contact layer: for a 4 ML thick LAO film, the spin polarization of the 2DEG decreases to $0.05/0.11\mu_B$ for IF/IF-1.

This spin polarization is a result of two effects. First, the fact that spin-up and spin-down Fermi levels at the surface and interface must be separately aligned (as well as with each other, finally). Second, a quantum confinement effect creates discrete bands, and a classical confinement effect leads to enhanced charge occupation at the IF and IF-1 layers.

As mentioned above, the magnetic moment of Ti in the surface contact layer is approximately $0.6\mu_B$ due to reduced coordination. This value decreases once the contact thickness is increased to 2 ML: the magnetic moment of the surface and subsurface Ti layer is reduced to $0.25\mu_B$ and $-0.05\mu_B$, respectively, owing to the enhanced Ti coordination. For other electrodes with lower surface magnetic moment, for example, 1 ML of Al (no magnetic moment) or 2 ML of Ti, the spin polarization of the 2DEG is quenched.

6. Broader functionalities of these interfacial systems

The range of unexpected phenomena that has been observed in these nanostructures has systematically been broadened by new discoveries. In the preceding sections, we have discussed how unusual properties, such as two-type carrier conduction or magnetism, may arise in these nanostructures. These theoretical studies are based, with a few exceptions, on atomically abrupt,

structurally ideal interfaces. It is understood that most (if not, all) samples are more complicated than this. We provide here an overview of the discoveries of magnetism at the interface, then of the reports of superconductivity and finally of the recent reports of coexistence of these two distinct, and usually strongly competing, types of long-range order. Understanding these phenomena will shed light on the underlying electronic structure at and near the interface. Specifically, several of these studies point out the importance of inhomogeneities in the samples, complications that should be kept in mind and will finally have to be taken into account. From the theorist's viewpoint, this emphasizes the importance of controlling defect concentration and distribution, to allow a closer connection of theory to experiment.

(*a*) *Hysteresis reflecting magnetic order*

Soon after the initial reports on conductivity in the LAO/STO system raised interest and research activity on this system, Brinkman *et al.* reported magnetic hysteresis in transport properties at the LAO/STO interface of PLD-deposited films [3]. This hysteresis, and an associated large negative magnetoresistance, reflects magnetic order arising at a few Kelvins and moves this oxide interface towards spintronics applications. Even prior to this study, the prospect of magnetism at this interface had been raised by Pentcheva & Pickett [63] in theoretical studies of LAO/STO superlattices with either n- or p-type interfaces. The question they faced at the time was this: at the polar LAO/STO interface, there is 0.5 carrier per interface cell too many (n-type) or too few (p-type) to fill bands. Therefore, the interface will be conducting unless other considerations come into play. For an n-type interface, it was demonstrated that correlation effects within GGA + U give rise to a charge and orbitally ordered state with magnetic moments of $0.7\mu_B$ at the Ti^{3+} sites. Later, Zhong & Kelly [64] investigated the effects of structural distortion beyond tetragonal symmetry and its impact on charge and spin ordering, finding an antiferromagnetic ground state. The relationship of the observed magnetism (due to Ti^{3+} local moments at the n-type interface) to the conduction by carriers remains to be clarified. We note that samples grown at high oxygen pressure, where the effect of oxygen vacancies is minimized, are nearly insulating with a sheet resistance that is seven orders of magnitude higher [3] than the initial samples studied by Ohtomo & Hwang [1]. On the other hand, the p-type interface had been found *always* to be non-conducting, independent of growth parameters. For a defect-free interface suggested by the initial reports, Pentcheva & Pickett proposed that correlation effects on the O 2p orbitals, resulting in charge order of oxygen holes with a magnetic moment $0.68\mu_B$, provided a plausible mechanism for insulating behaviour. While this is an interesting case of d^0-magnetism, the insulating behaviour of the p-type interface has been generally ascribed to O vacancies [35].

The possibility of magnetism at these interfaces was highlighted in *Physics Today* in 2007 [65], and remains an enigma. Magnetism was further discussed by Huijben *et al.* [17], who provided a broader overview of work on oxide interfaces up to that time. Subsequently, Seri & Klein [66] reported antisymmetric magnetoresistance at this interface, and noted magnetic-field-induced inhomogeneous magnetism, but did not characterize it as spontaneous ferromagnetism. Ariando *et al.* [67] detected dia-, ferro- and paramagnetic signals

interpreted in terms of phase separation. In particular, the ferromagnetic phase persisted beyond room temperature. Li *et al.* [6] reported magnetic effects persisting up to 200 K, which raises new questions, beginning with how such apparently weak magnetism can maintain spin order to such high temperatures.

(*b*) *Superconductivity*

The observation of superconductivity at the n-type interface by Reyren *et al.* [2] further enriched the variety of phenomena that have been reported. The superconducting state in PLD-grown samples at intermediate pressures (10^{-4} mbar) arose below 200 mK. Because bulk n-type STO superconducts in that range (up to 400 mK), one might initially question how new the phenomenon really is. The magnetic field directional dependence established that the superconductivity was highly two dimensional, and so in that manner, its behaviour is quite unlike that of bulk STO; as a 2D system, it is characterized by a 2D carrier concentration rather than a three-dimensional (3D) one. As with the magnetism, the degree of localization around the interface, and origin and character of the carriers, have become objects of scrutiny.

Subsequent reports by Caviglia *et al.* [68] and Ben Shalom *et al.* [69] confirmed superconductivity arising at this interfacial system. The latter report, where 15 unit cells of LAO were deposited with a pulsed laser and the carrier density was varied with gating, mapped out a portion of the phase diagram where T_c decreases as the carrier density increases. Kim *et al.* [70] studied, by Shubnikov-de Haas oscillations, the (presumably) related superconducting state in δ-doped STO films deposited by PLD. The doping by Nb (for Ti) was performed in a varying number of TiO_2 layers, and a 2D to 3D crossover in the superconducting state was monitored. This still very new topic of oxide interface superconductivity has been reviewed by Gariglio & Triscone [71]

(*c*) *Coexistence*

Historically, magnetism and superconductivity were mutual anathema, but the high-temperature superconductivity discovered in cuprates changed that. The latest big discovery in superconductivity, the Fe-based pnictides and chalcogenides also display magnetic phases next to superconducting ones. These, as well as some other materials classes such as heavy fermion metals [72], raise questions about possible connections between these ordered phases. In these examples, the magnetism is antiferromagnetism (or correlations). Superconductivity coexisting with *ferromagnetism* is very rare, having been reported only in the past decade or so in $RuSr_2GdCu_2O_8$ [73] and in the three uranium compounds UGe_2, URhGe and UCoGe. Aoki *et al.* have provided a recent overview summarizing several of the phenomena and some of the issues to account for observations [74]. There are several challenges to be overcome for superconductivity to arise in a ferromagnet (see discussion in Pickett *et al.* [75]): exchange splitting of up and down bands that disrupts pairing, magnetic field disruption of superconducting order, etc. In the following, we return briefly to some of these issues.

The first observation of coexistence by Dikin *et al.* [5] involved superconducting onsets around $T_c \approx 150$ mK on PLD films of 10 unit cells of LAO on TiO_2-terminated STO(001) substrates. They observed hysteresis in $T_c(H)$ curves

(H is the magnetic field) attributed to underlying ferromagnetic order. Their interpretation focuses on two parallel conduction channels: one consists of localized, magnetic states that are intrinsic to the interface (*viz.* Ti^{3+} moments, likely in the immediate interface region), while the other carriers are itinerant electrons contributed by defects (a likely candidate being oxygen vacancies). While previous reports indicated quenching of magnetism at a few Kelvin, Li *et al.* [6] report high-resolution magnetic torque magnetometry measurements, showing evidence of magnetic ('superparamagnetic-like') order up to 200 K. The superconducting signal in their samples arises below 120 mK.

Most recently, Bert *et al.* [4] provided a real space picture of their PLD grown films. They performed imaging with a scanning superconducting quantum interference device (SQUID) over $\sim 200\,\mu m$ square regions on samples of 10 ML LAO on STO(001) substrates. They report strong inhomogeneity, with sub-micron regions of ferromagnetism in a background of paramagnetic carriers that show a diamagnetic superconducting signal around 100 mK; thus, superconductivity and magnetism coexist in the sample, but not in the same region. For comparison, no magnetic dipoles were observed in a reference sample of δ-doped STO. From their transport and thermodynamic measurements, they infer that most of the intrinsic carriers ($4 \times 10^{14}\,cm^{-2}$ per interface cell for an atomically perfect interface) are localized because an order-of-magnitude fewer carriers contribute to the Hall conductivity.

Some early attempts to account for this coexistence have appeared [44,76,77]. The coexistence seems an even more delicate question here than in the ferromagnetic superconductors mentioned earlier. The ~ 200 mK critical temperature reflects a Bardeen–Cooper–Schrieffer gap of a few μeV, a truly tiny energy scale that appreciable exchange splitting of the bands would overwhelm. The critical magnetic field should be very small. There are aspects of the interfaces that suggest the means to avoid these pair breakers. The magnetic electrons and the superconducting carriers may reside in different bands, requiring a generalization of models applied to the previously known ferromagnetic superconductors. Inhomogeneity or phase separation may play a role, and coexistence in the same sample may not imply local coexistence (in the same region of the sample). The superconducting state may be inhomogeneous of the Fulde–Farrel–Larkin–Ovchinnikov type [78,79].

7. Summary

The LAO/STO system shows a remarkable spectrum of electronic phenomena, some of which seem to be understood and others require further study. We have provided an overview on the basis of DFT results addressing how the electrostatic boundary conditions determine charge (re-)distribution and the electronic state. A variety of parameters are identified (such as the surface and interface termination and stoichiometry, the presence of metallic or oxide overlayers, as well as defects and adsorbates) that enable tuning the electronic behaviour of this system. Understanding and controlling these parameters, and especially defects, dopants [80] and adsorbates, remain a challenging area that needs further attention in future theoretical and experimental studies.

We acknowledge financial support through the DFG SFB/TR80 (project C3) and grant h0721 for computational time at the Leibniz Computational Center Garching. V.G.R. acknowledges financial support from CONACYT (Mexico) and DAAD (Germany). W.E.P. was supported by U.S. Department of Energy grant no. DE-FG02-04ER46111.

References

1 Ohtomo, A. & Hwang, H. Y. 2004 A high-mobility electron gas at the $LaAlO_3/SrTiO_3$ heterointerface. *Nature* **427**, 423–426. (doi:10.1038/nature02308)
2 Reyren, N. *et al.* 2007 Superconducting interfaces between insulating oxides. *Science* **317**, 1196–1199. (doi:10.1126/science.1146006)
3 Brinkman, A. *et al.* 2007 Magnetic effects at the interface between non-magnetic oxides. *Nature Mater.* **6**, 493–496. (doi:10.1038/nmat1931)
4 Bert, J. A., Kalisky, B., Bell, C., Kim, M., Hikita, Y., Hwang, H. Y. & Moler, K. A. 2011 Direct imaging of the coexistence of ferromagnetism and superconductivity at the $LaAlO_3/SrTiO_3$ interface. *Nat. Phys.* **7**, 767–771. (doi:10.1038/nphys2079)
5 Dikin, D. A., Mehta, M., Bark, C. W., Folkman, C. M., Eom, C. B. & Chandrasekhar, V. 2011 Coexistence of superconductivity and ferromagnetism in two dimensions. *Phys. Rev. Lett.* **107**, 056802. (doi:10.1103/PhysRevLett.107.056802)
6 Li, L., Richter, C., Mannhart, J. & Ashoori, R. C. 2011 Coexistence of magnetic order and two-dimensional superconductivity at $LaAlO_3/SrTiO_3$ interfaces. *Nat. Phys.* **7**, 762–766. (doi:10.1038/nphys2080)
7 Thiel, S., Hammerl, G., Schmehl, A., Schneider, C. W. & Mannhart, J. 2006 Tunable quasi-two-dimensional electron gases in oxide heterostructures. *Science* **313**, 1942–1945. (doi:10.1126/science.1131091)
8 Cen, C., Thiel, S., Hammerl, G., Schneider, C. W., Andersen, K. E., Hellberg, C. S., Mannhart, J. & Levy, J. 2008 Nanoscale control of an interfacial metal-insulator transition at room temperature. *Nat. Mater.* **7**, 298–302. (doi:10.1038/nmat2136)
9 Bi, F., Bogorin, D. F., Cen, C., Bark, C. W., Park, J. W., Eom, C. B. & Levy, J. 2010 'Water-cycle' mechanism for writing and erasing nanostructures at the $LaAlO_3/SrTiO_3$ interface. *Appl. Phys. Lett.* **97**, 173110. (doi:10.1063/1.3506509)
10 Chen, Y. Z., Zhao, J. L., Sun, J. R., Pryds, N. & Shen, B. G. 2010 Resistance switching at the interface of $LaAlO_3/SrTiO_3$. *Appl. Phys. Lett.* **97**, 123102. (doi:10.1063/1.3490646)
11 Cen, C., Thiel, S., Mannhart, J. & Levy, J. 2009 Oxide nanoelectronics on demand. *Science* **323**, 1026–1030. (doi:10.1126/science.1168294)
12 Bogorin, D. F., Irvin, P., Cen, C. & Levy, J. 2010 $LaAlO_3/SrTiO_3$-based device concepts. (http://arxiv.org/abs/1011.5290)
13 Pentcheva, R. *et al.* 2010 Parallel electron-hole bilayer conductivity from electronic interface reconstruction. *Phys. Rev. Lett.* **104**, 166804. (doi:10.1103/PhysRevLett.104.166804)
14 Hwang, H. Y. 2006 Tuning interface states. *Science* **313**, 1895–1896. (doi:10.1126/science.1133138)
15 Goniakowski, J., Finocchi, F. & Noguera, C. 2008 Polarity of oxide surfaces and nanostructures. *Rep. Prog. Phys.* **71**, 016501. (doi:10.1088/0034-4885/71/1/016501)
16 Pauli, S. A. & Willmott, P. R. 2008 Conducting interfaces between polar and non-polar insulating perovskites. *J. Phys., Condens. Matter* **20**, 264012. (doi:10.1088/0953-8984/20/26/264012)
17 Huijben, M., Brinkman, A., Koster, G., Rijnders, G., Hilgenkamp, H. & Blank, D. H. A. 2009 Structure–property relation of $SrTiO_3/LaAlO_3$ interfaces. *Adv. Mater.* **21**, 1665–1677. (doi:10.1002/adma.200801448)
18 Pentcheva, R. & Pickett, W. E. 2010 Electronic phenomena at complex oxide interfaces: insights from first principles. *J. Phys., Condens. Matter* **22**, 043001. (doi:10.1088/0953-8984/22/4/043001)
19 Chen, H., Kolpak, A. M. & Ismail-Beigi, S. 2010 Electronic and magnetic properties of $SrTiO_3/LaAlO_3$ interfaces from first principles. *Adv. Mater.* **22**, 2881–2899. (doi:10.1002/adma.200903800)

20 Zubko, P., Gariglio, S., Gabay, M., Ghosez, P. & Triscone, J. M. 2011 Interface physics in complex oxide heterostructures. *Annu. Rev. Condens. Matter Phys.* **2**, 141–165. (doi:10.1146/annurev-conmatphys-062910-140445)

21 Stengel, M. 2011 First-principles modeling of electrostatically doped perovskite systems. *Phys. Rev. Lett.* **106**, 136803. (doi:10.1103/PhysRevLett.106.136803)

22 Xie, Y., Bell, C., Yajima, T., Hikita, Y. & Hwang, H. Y. 2010 Charge writing at the $LaAlO_3/SrTiO_3$ surface. *Nano Lett.* **10**, 2588–2591. (doi:10.1021/nl1012695)

23 Segal, Y., Ngai, J. H., Reiner, J. W., Walker, F. J. & Ahn, C. H. 2009 X-ray photoemission studies of the metal-insulator transition in $LaAlO_3/SrTiO_3$ structures grown by molecular beam epitaxy. *Phys. Rev. B* **80**, 241107. (doi:10.1103/PhysRevB.80.241107)

24 Sing, M. *et al.* 2009 Profiling the interface electron gas of $LaAlO_3/SrTiO_3$ heterostructures with hard X-ray photoelectron spectroscopy. *Phys. Rev. Lett.* **102**, 176805. (doi:10.1103/PhysRevLett.102.176805)

25 Chambers, S. *et al.* 2010 Instability, intermixing and electronic structure at the epitaxial heterojunction. *Surf. Sci. Rep.* **65**, 317–352. (doi:10.1016/j.surfrep.2010.09.001)

26 Zhong, Z., Xu, P. X. & Kelly, P. J. 2010 Polarity-induced oxygen vacancies at $LaAlO_3/SrTiO_3$ interfaces. *Phys. Rev. B* **82**, 165127. (doi:10.1103/PhysRevB.82.165127)

27 Bristowe, N. C., Littlewood, P. B. & Artacho, E. 2011 Surface defects and conduction in polar oxide heterostructures. *Phys. Rev. B* **83**, 205405. (doi:10.1103/PhysRevB.83.205405)

28 Son, W., Cho, E., Lee, J. & Han, S. 2010 Hydrogen adsorption and carrier generation in $LaAlO_3$–$SrTiO_3$ heterointerfaces: a first-principles study. *J. Phys., Condens. Matter* **22**, 315501. (doi:10.1088/0953-8984/22/31/315501)

29 Willmott, P. R. *et al.* 2007 Structural basis for the conducting interface between $LaAlO_3$ and $SrTiO_3$. *Phys. Rev. Lett.* **99**, 155502. (doi:10.1103/PhysRevLett.99.155502)

30 Qiao, L., Droubay, T. C., Shutthanandan, V., Zhu, Z., Sushko, P. V. & Chambers, S. A. 2010 Thermodynamic instability at the stoichiometric $LaAlO_3/SrTiO_3(001)$ interface. *J. Phys., Condens. Matter* **22**, 312201. (doi:10.1088/0953-8984/22/31/312201)

31 Ishibashi, S. & Terakura, K. 2008 Analysis of screening mechanisms for polar discontinuity for $LaAlO_3/SrTiO_3$ thin films based on *ab initio* calculations. *J. Phys. Soc. Jpn.* **77**, 104706. (doi:10.1143/JPSJ.77.104706)

32 Pentcheva, R. & Pickett, W. E. 2009 Avoiding the polarization catastrophe in $LaAlO_3$ overlayers on $SrTiO_3(001)$ through polar distortion. *Phys. Rev. Lett.* **102**, 107602. (doi:10.1103/PhysRevLett.102.107602)

33 Son, W.-J., Cho, E., Lee, B., Lee, J. & Han, S. 2009 Density and spatial distribution of charge carriers in the intrinsic *n*-type $LaAlO_3$–$SrTiO_3$ interface. *Phys. Rev. B* **79**, 245411. (doi:10.1103/PhysRevB.79.245411)

34 Pauli, S. A. *et al.* 2011 Evolution of the interfacial structure of $LaAlO_3$ on $SrTiO_3$. *Phys. Rev. Lett.* **106**, 036101. (doi:10.1103/PhysRevLett.106.036101)

35 Nakagawa, N., Hwang, H. Y. & Muller, D. A. 2006 Why some interfaces cannot be sharp. *Nat. Mater.* **5**, 204–209. (doi:10.1038/nmat1569)

36 Pavlenko, N. & Kopp, T. 2004 Structural relaxation and metal-insulator transition at the interface between $SrTiO_3$ and $LaAlO_3$. *Surf. Sci.* **605**, 1114–1121. (doi:10.1016/j.susc.2011.03.016)

37 Huijben, M., Rijnders, G., Blank, D. H. A., Bals, S., Van Aert, S., Verbeeck, J., Van Tendeloo, G., Brinkman, A. & Hilgenkamp, H. 2006 Electronically coupled complementary interfaces between perovskite band insulators. *Nat. Mater.* **5**, 556–560. (doi:10.1038/nmat1675)

38 Padilla, J. & Vanderbilt, D. 1998 *Ab initio* study of $SrTiO_3$ surfaces. *Surf. Sci.* **418**, 64–70. (doi:10.1016/S0039-6028(98)00670-0)

39 Kimura, S., Yamauchi, J., Tsukada, M. & Watanabe, S. 1995 First-principles study on electronic structure of the (001) surface of $SrTiO_3$. *Phys. Rev. B* **51**, 11 049–11 054. (doi:10.1103/PhysRevB.51.11049)

40 Takizawa, M., Tsuda, S., Susaki, T., Hwang, H. Y. & Fujimori, A. 2011 Electronic charges and electric potential at $LaAlO_3/SrTiO_3$ interfaces studied by core-level photoemission spectroscopy. *Phys. Rev. B* **84**, 245124. (doi:10.1103/PhysRevB.84.245124)

41 Chen, H., Kolpak, A. M. & Ismail-Beigi, S. 2009 Fundamental asymmetry in interfacial electronic reconstruction between insulating oxides: an *ab initio* study. *Phys. Rev. B* **79**, 161402. (doi:10.1103/PhysRevB.79.161402)

42 Zhang, L., Zhou, X. F., Wang, H. T., Xu, J. J., Li, J., Wang, E. G. & Wei, S. H. 2010 Origin of insulating behavior of the *p*-type $LaAlO_3/SrTiO_3$ interface: polarization-induced asymmetric distribution of oxygen vacancies. *Phys. Rev. B* **82**, 125412. (doi:10.1103/PhysRevB.82.125412)

43 Li, Y., Na Phattalung, S., Limpijumnong, S., Kim, J. & Yu, J. 2009 Formation of oxygen vacancies and charge carriers induced in the *n*-type interface of a $LaAlO_3$ overlayer on $SrTiO_3$(001) *Phys. Rev. B* **84**, 245307. (doi:10.1103/PhysRevB.84.245307)

44 Pavlenko, N., Kopp, T., Tsymbal, E. Y., Sawatzky, G. A. & Mannhart, J. 2012 Magnetic and superconducting phases at the $LaAlO_3/SrTiO_3$ interface: the Ti 3d interface electrons. *Phys. Rev. B* **85**, 020407. (doi:10.1103/PhysRevB.85.020407)

45 Perdew, J. P., Burke, K. & Ernzerhof, M. 1996 Generalized gradient approximation made simple. *Phys. Rev. Lett.* **77**, 3865–3868. (doi:10.1103/PhysRevLett.77.3865)

46 Jany, R. *et al.* 2010 Diodes with breakdown voltages enhanced by the metal-insulator transition of $LaAlO_3$–$SrTiO_3$ interfaces. *Appl. Phys. Lett.* **96**, 183504. (doi:10.1063/1.3428433)

47 Singh-Bhalla, G., Bell, C., Ravichandran, J., Siemons, W., Hikita, Y., Salahuddin, S., Hebard, A. F., Hwang, H. Y. & Ramesh, R. 2011 Built-in and induced polarization across $LaAlO_3/SrTiO_3$ heterojunctions. *Nat. Phys.* **7**, 80–86. (doi:10.1038/NPHYS1814)

48 Campbell, C. T. 1997 Ultrathin metal films and particles on oxide surfaces: structural, electronic and chemisorptive properties. *Surf. Sci. Rep.* **27**, 1–111. (doi:10.1016/S0167-5729(96)00011-8)

49 Goniakowski, J. & Noguera, C. 2004 Electronic states and Schottky barrier height at metal/MgO(100) interfaces. *Interf. Sci.* **12**, 93–103. (doi:10.1023/B:INTS.0000012298.34540.50)

50 Duan, C. G., Jaswal, S. S. & Tsymbal, E. Y. 2006 Predicted magnetoelectric effect in $Fe/BaTiO_3$ multilayers: ferroelectric control of magnetism. *Phys. Rev. Lett.* **97**, 047201. (doi:10.1103/PhysRevLett.97.047201)

51 Fu, Q. & Wagner, T. 2007 Interaction of nanostructured metal overlayers with oxide surfaces. *Surf. Sci. Rep.* **62**, 431–498. (doi:10.1016/j.surfrep.2007.07.001)

52 Fechner, M., Maznichenko, I. V., Ostanin, S., Ernst, A., Henk, J., Bruno, P. & Mertig, I. 2008 Magnetic phase transition in two-phase multiferroics predicted from first principles. *Phys. Rev. B* **78**, 212406. (doi:10.1103/PhysRevB.78.212406)

53 Arras, R., Ruiz, V. G., Pickett, W. E. & Pentcheva, R. 2012 Tuning the two-dimensional electron gas at the $LaAlO_3/SrTiO_3$(001) interface by metallic contacts. *Phys. Rev. B* **85**, 125404. (doi:10.1103/PhysRevB.85.125404)

54 Blaha, P., Schwarz, K., Madsen, G., Kvasnicka, D. & Luitz, J. 2001 *WIEN2k, an augmented plane wave plus local orbitals program for calculating crystal properties*. Technische Universität Wien, Austria: Karlheinz Schwarz.

55 Anisimov, V. I., Solovyev, I. V., Korotin, M. A., Czyżyk, M. T. & Sawatzky, G. A. 1993 Density-functional theory and NiO photoemission spectra. *Phys. Rev. B* **48**, 16 929–16 934. (doi:10.1103/PhysRevB.48.16929)

56 Asthagiri, A. & Sholl, D. S. 2006 Pt thin films on the polar $LaAlO_3$(100) surface: a first-principles study. *Phys. Rev. B* **73**, 125432. (doi:10.1103/PhysRevB.73.125432)

57 Asthagiri, A. & Scholl, D. S. 2002 First principles study of Pt adhesion and growth on SrO- and TiO_2-terminated $SrTiO_3$(100). *J. Chem. Phys.* **116**, 9914–9925. (doi:10.1063/1.1476322)

58 Ochs, T., Köstlmeier, S. & Elsässer, C. 2001 Microscopic structure and bonding at the $Pd/SrTiO_3$ (001) interface an ab-initio local-density-functional study. *Integr. Ferroelectr.* **32**, 267–278. (doi:10.1080/10584580108215697)

59 Oleinik, I. I., Tsymbal, E. Y. & Pettifor, D. G. 2001 Atomic and electronic structure of $Co/SrTiO_3/Co$ magnetic tunnel junctions. *Phys. Rev. B* **65**, 020401. (doi:10.1103/PhysRevB.65.020401)

60 Okamoto, S., Millis, A. J. & Spaldin, N. A. 2006 Lattice relaxation in oxide heterostructures: $LaTiO_3/SrTiO_3$ superlattices. *Phys. Rev. Lett.* **97**, 056802. (doi:10.1103/PhysRevLett.97.056802)

61 Pentcheva, R. & Pickett, W. E. 2008 Ionic relaxation contribution to the electronic reconstruction at the n-type $LaAlO_3/SrTiO_3$ interface. *Phys. Rev. B* **78**, 205106. (doi:10.1103/PhysRevB.78.205106)
62 Stengel, M., Vanderbilt, D. & Spaldin, N. A. 2009 Enhancement of ferroelectricity at metal-oxide interfaces. *Nat. Mater.* **8**, 392–397. (doi:10.1038/NMAT2429)
63 Pentcheva, R. & Pickett, W. E. 2006 Charge localization or itineracy at $LaAlO_3/SrTiO_3$ interfaces: hole polarons, oxygen vacancies, and mobile electrons. *Phys. Rev. B* **74**, 035112. (doi:10.1103/PhysRevB.74.035112)
64 Zhong, Z. & Kelly, P. 2008 Electronic-structure-induced reconstruction and magnetic ordering at the $LaAlO_3/SrTiO_3$ interface. *Europhys. Lett.* **84**, 27001. (doi:10.1209/0295-5075/84/27001)
65 Goss Levi, B. 2007 Interface between nonmagnetic insulators may be ferromagnetic and conducting. *Phys. Today* **60**, 23. (doi:10.1063/1.2754590)
66 Seri, S. & Klein, L. 2009 Antisymmetric magnetoresistance of the $SrTiO_3/LaAlO_3$ interface. *Phys. Rev. B* **80**, 180410. (doi:10.1103/PhysRevB.80.180410)
67 Ariando *et al.* 2011 Electronic phase separation at the $LaAlO_3/SrTiO_3$ interface. *Nature Commun.* **2**, 188. (doi:10.1038/ncomms1192)
68 Caviglia, A. D. *et al.* 2008 Electric field control of the $LaAlO_3/SrTiO_3$ interface ground state. *Nature* **456**, 624–627. (doi:10.1038/nature07576)
69 Ben Shalom, M., Sachs, M., Rakhmilevitch, D., Palevski, A. & Dagan, Y. 2010 Tuning spin-orbit coupling and superconductivity at the $SrTiO_3/LaAlO_3$ interface: a magnetotransport study. *Phys. Rev. Lett.* **104**, 126802. (doi:10.1103/PhysRevLett.104.126802)
70 Kim, M., Bell, C., Kozuka, Y., Kurita, M., Hikita, Y. & Hwang, H. Y. 2011 Fermi surface and superconductivity in low-density high-mobility δ-doped $SrTiO_3$. *Phys. Rev. Lett.* **107**, 106801. (doi:10.1103/PhysRevLett.107.106801)
71 Gariglio, S. & Triscone, J. M. 2011 Oxide interface superconductivity. *C. R. Phys.* **12**, 591–599. (doi:10.1016/j.crhy.2011.03.006)
72 Sarrao, J. L. *et al.* 2002 Plutonium-based superconductivity with a transition temperature above 18 K. *Nature* **420**, 297–299. (doi:10.1038/nature01212)
73 Bernhard, C. 1999 Coexistence of ferromagnetism and superconductivity in the hybrid ruthenate-cuprate compound $RuSr_2GdCu_2O_8$ studied by muon spin rotation and DC magnetization. *Phys. Rev. B* **59**, 14099–14107. (doi:10.1103/PhysRevB.59.14099)
74 Aoki, D., Hardy, F., Miyake, A., Taufour, V., Matsuda, T. D. & Flouquet, J. 2011 Properties of ferromagnetic superconductors. *C. R. Phys.* **12**, 573–583. (doi:10.1016/j.crhy.2011.04.007)
75 Pickett, W. E., Weht, R. & Shick, A. B. 1999 Superconductivity in ferromagnetic $RuSr_2GdCu_2O_8$. *Phys. Rev. Lett.* **83**, 3713–3716. (doi:10.1103/PhysRevLett.83.3713)
76 Michaeli, K., Potter, A. C. & Lee, P. A. 2012 Superconductivity and ferromagnetism in oxide interface structures: possibility of finite momentum pairing. *Phys. Rev. Lett.* **108**, 117003. (doi:10.1103/PhysRevLett.108.117003)
77 Stephanos, C., Kopp, T., Mannhart, J. & Hirschfeld, P. J. 2011 Interface-induced d-wave pairing. *Phys. Rev. B* **84**, 100510. (doi:10.1103/PhysRevB.84.100510)
78 Fulde, P. & Ferrell, R. A. 1964 Superconductivity in a strong spin-exchange field. *Phys. Rev.* **135**, A550–A563. (doi:10.1103/PhysRev.135.A550)
79 Larkin, A. I. & Ovchinnikov, Y. N. 1964 *Zh. Eksp. Teor. Fiz*, **47**, 1136–1146.
80 Fix, T., Schoofs, F., MacManus-Driscoll, J. L. & Blamire, M.G. 2009 Charge confinement and doping at $LaAlO_3/SrTiO_3$ interfaces. *Phys. Rev. Lett.* **103**, 166802. (doi:10.1103/PhysRevLett.103.166802)